ChemPubSoc Europe
DOI: 10.1002/cplu.201500293
CHEMPLUSCHEM
Full Papers

Chitin-Derived Mesoporous, Nitrogen-Containing Carbon for Heavy-Metal Removal and Styrene Epoxidation

Yongjun Gao, Xi Chen, Jiaguang Zhang, and Ning Yan*[a]

The production of a series of mesoporous, nitrogen-containing (N-containing) carbon materials directly from pure chitin by means of carbonization at different temperatures under template-free conditions is reported. Thermogravimetric analysis combined with infrared spectroscopy was applied to follow the temperature-dependent chemical events during the carbonization process, thereby shedding light on the automated pore formation mechanism. The physicochemical properties of the N-containing carbon materials have been extensively investigated, which provided guidance and rational understanding of the application of these materials. It was found that the N-containing carbon materials obtained at lower temperatures (400–600 °C) were enriched with amine, amide, and pyrrolic functionalities, which enables their very high efficiency as adsorbents to remove toxic heavy metals, such as Cr^{VI}, Hg^{II}, and Pd^{II}, from water. In contrast, N-containing carbon materials prepared at higher temperatures (800–1000 °C) were enriched with graphitic N, which exhibited excellent catalytic activity in the epoxidation of styrene.

Introduction

Mesoporous carbon materials, which possess a high surface area, large pore volume, and special physicochemical properties,[1] have been widely applied in the fields of adsorbents,[2] fuel cells,[3] gas separation and storage,[4] and catalysis.[5] To improve the performance of mesoporous carbon materials, surface functionality incorporation and heteroatom doping are often used.[3] Generally, the introduction of nitrogen atoms to the carbon matrix not only adjusts the surface polarity and electron-donor ability, but also influences its neighboring carbon atoms leading to improved properties.[6] And the introduction of nitrogen atoms into the carbon framework can enhance the adsorption capacity and catalytic performance. The synthesis of N-containing carbon materials commonly includes carbonizing N-containing precursors (such as N-containing ionic liquids,[7] amino sugar,[8] melamine,[9] N-containing polymer[10]), or treating pre-synthesized carbon materials with N-containing compounds (such as ammonia[11] or acetonitrile[12]). Despite the considerable advances in the field, the current protocols for the manufacture of N-containing, porous carbon have some limitations. First of all, the nitrogen source is often based on non-renewable and/or toxic chemicals, which is not compatible with the principles of green chemistry.[13] In addition, template agents are commonly needed to obtain mesoporous structures. Some of the templates have to be chemically corroded after the carbonization, which leads to increased synthetic complexity and enhanced product cost. Finally, some methods lack the tunability to modify the nitrogen content and the types of N-containing groups on the surface, which limits the scope of application.

Chitin, the second most abundant biopolymer on earth, is a N-containing biomass material existing in the exoskeletons of insects and crustaceans.[14] Chitin has long been considered as a starting material for the production of functional polymers.[15] Apart from that, it finds little application. Indeed, the vast majority of the waste chitin material is either dumped back into the sea or transported to special landfills without utilization.[16] Considering the biologically fixed 7 wt % nitrogen (see Table 1 for the chemical structure), chitin provides a cheap and renewable resource to synthesize N-containing chemicals and materials. Very recently, the transformation of chitin into a series of chemicals has been conducted, but the product yields were typically low.[17] Simple, effective, and value-added transformation of chitin into chemicals and materials, in particular those containing nitrogen, is highly desirable.

There are several previous studies pertinent to the transformation of chitin to N-containing carbon materials. Prawn shells[18] and crawfish shell[19] were carbonized at 750 °C to generate N-doped porous carbon/$CaCO_3$ composites, as well as purified porous carbon upon removal of $CaCO_3$ by an acid. In another study, chitin was heated to temperatures between 170 and 450 °C, and the resulting biochar was used to absorb polycyclic aromatic hydrocarbons.[20] Chitin was also transformed into N-containing carbon materials following a three-step procedure including sequential deacetylation, hydrolysis, and finally carbonization.[8] In this latter study, the real precursor is the partially deacetylated chitosan instead of chitin. 13–36 wt %

---

[a] Dr. Y. Gao, X. Chen, Dr. J. Zhang, Prof. Dr. N. Yan
Department of Chemical and Biomolecular Engineering
National University of Singapore
4 Engineering Drive 4, 117585 Singapore (Singapore)
E-mail: ning.yan@nus.edu.sg

Supporting information for this article is available on the WWW under http://dx.doi.org/10.1002/cplu.201500293.

Part of a Special Issue to celebrate Singapore's Golden Jubilee. To view the complete issue, visit: http://dx.doi.org/10.1002/cplu.v80.8.

Table 1. Carbonization yields and elements analysis of various NC products.

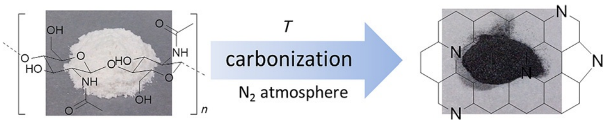

Products	Mass yield [wt %]	XPS results [wt %]			Elemental analyzer results [wt %]			
		C	N	O	C	N	H	O[a]
chitin	–	54.2	5.0	40.8	47.24	6.89	6.40	39.5
NC-400	22.0	78.9	8.4	12.7	73.08	8.87	4.64	13.4
NC-600	18.6	86.7	5.0	8.3	81.87	7.45	2.49	8.19
NC-800	18.1	88.0	5.1	6.9	82.94	7.09	1.70	8.27
NC-1000	18.3	90.2	3.1	6.7	88.29	4.75	1.33	5.63

[a] The oxygen content is calculated based on the formula: 100−C (wt %)−H (wt %)−N (wt %).

$Si(OCH_3)_4$ was used as a co-template and was removed with NaOH after carbonization at 900 °C. From these, it can be seen that chitin is a promising starting material for N-containing carbon materials, but several important issues remain to be addressed. Only one study starting with pure chitin for carbonization was carried out.[20] Moreover, there has been no systematic, thorough study on the structure–carbonization temperature relationship at a practically useful temperature range (400–1000 °C) for chitin-derived N-containing carbon materials. Subsequently, the inadequate understanding of the structural features of N-containing carbon materials obtained at different temperatures hampers diversified, wide application of these materials as a rational choice. With this in mind, we tested the production of N-containing mesoporous carbon materials directly from chitin under template-free conditions at four different carbonization temperatures. This resulted in N-containing carbon materials with different surface areas, nitrogen content, and surface functionalities. They exhibited excellent performance in the removal of heavy metals such as Cr^{VI}, Pb^{II}, and Hg^{II} from water, and in the epoxidation of styrene.

Results and Discussion

Preparation of N-containing carbon materials from chitin

Chitin extracted from different sources has different crystal structures and different thermal stability. In our study, α-chitin was employed throughout. The carbonization of chitin under nitrogen was firstly followed by on-line thermogravimetry coupled with Fourier transform infrared spectroscopy (TG-IR Figure 1). In TG analysis (Figure 1a), there are three weight-loss stages during the entire heating process. The first stage ranges from the starting temperature to 140 °C with a weight loss of 1.1 wt %, which reflects the evaporation of the remaining water. The second stage is between about 300 and 450 °C, with a significant loss of 78.3 wt % and an associated exothermic peak centered at 431 °C on the differential thermal analysis (DTA) curve, which corresponds to the decomposition of chitin.

The gas products as well as the low-boiling-point products evolved during the degradation of chitin were detected by FTIR spectroscopy (Figure 1b). According to the contour, a large peak at 1773 cm^{-1} was observed firstly, which suggests the generation of carbonyl-group-containing compounds. This peak, together with the C–O stretching vibration peak at 1170 cm^{-1} and the O–H stretching vibration peak at around 3000 cm^{-1},[21] suggested the formation of carboxylic acids. Slightly afterwards, a small peak located at 2145 cm^{-1} and a moderate peak located at 2352 cm^{-1} were detected, which corresponded to CO and CO_2, respectively.[21] In addition, a peak at 1511 cm^{-1} ascribed to the N=O stretching vibration and the O–H characteristic vibration of water at 3729 cm^{-1} were detected. Therefore, the weight loss at the second stage was attributed to the degradation of the polymeric saccharide, including the deacetylation of chitin, followed by decomposition of the deacetylated pyranose rings, during which some nitrogen was lost in the form of nitrogen oxide. In fact, some organic nitrogen-containing compounds were also generated from chitin, such as acetamide and 3-hydroxypyridine (see below). However, these compounds were not detected by FTIR spectroscopy, presumably owing to their low concentration. The third weight-loss stage is from 450 to 870 °C but the weight loss is insignificant,

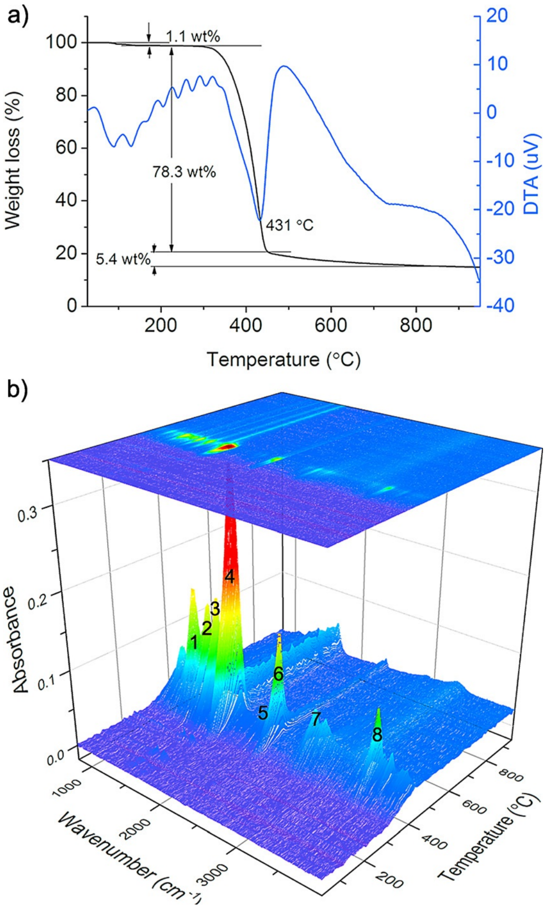

Figure 1. (a) TGA and DTA curves and (b) three-dimensional on-line FTIR spectra of the volatile products in chitin carbonization. The labeled peaks in the FTIR spectrum represent: (1) C–O stretching, (2) O–H bending, (3) N–H bending, (4) C=O stretching, (5) CO, (6) CO_2, (7) C–H stretching, and (8) O–H stretching.

which may result from the decomposition of surface functional groups. At this stage, there is no new peak appearing on the FTIR spectrum. From TG-IR analysis, the decomposition of chitin mainly occurred between 300 and 450 °C and generated a large amount of volatile products that were detected in the system until the end of the analysis. Based on the TG analysis of chitin, we selected 400 °C as the minimal temperature to study the carbonization of chitin in a nitrogen atmosphere.

The method for preparing N-containing carbon materials is extremely simple. Briefly, chitin carbonization is conducted in a tubular furnace in a nitrogen atmosphere under temperature-programmed heating (10 °C min^{-1}) that is maintained for four hours after reaching the desired temperature. Chitin was carbonized at 400, 600, 800, and 1000 °C, and the products were termed as NC-400, NC-600, NC-800, and NC-1000, respectively. Table 1 shows the carbon-product mass yields at different carbonization temperatures. From X-ray photoelectron spectroscopy (XPS) analysis it can be seen that the carbon content increased monotonically (from 82.5 to 90.2 wt %), whereas the oxygen (from 12.7 to 6.7 wt %) and nitrogen (from 8.4 to 3.1 wt %) contents decreased with the increase of temperature, which indicated the decomposition of O- and N-containing groups on the surface at high temperature. The contents of carbon, nitrogen, and hydrogen in these materials were also analyzed by an elemental analyzer. The nitrogen content in NC-400 (8.87 wt %) is higher than that in chitin (6.89 wt %), and decreased only slightly from 400 to 800 °C. Even when treated at 1000 °C, a significant portion of nitrogen was maintained in the bulk (4.75 wt %). In addition, a large amount of liquid product (about 35–50 wt %) can be generated and collected at the exit of the quartz tube. Analysis of the liquid product obtained at 600 °C by gas chromatography-mass spectrometry (GC-MS) and high-performance liquid chromatography (HPLC) revealed acetic acid and acetamide to be the two main products with yields of 5.9 and 2.2 wt %, respectively. Ethylene glycol, glycolic acid, 3-hydroxypyridine, and *N*-acetylglucosamine were also detected but the yields were much lower (combined yield: 1.5 wt %). From mass balance measurements, 30–40 wt % products were in the form of gases (CO, CO_2, etc.).

Structure characterization

To further probe the structural changes during carbonization, X-ray diffraction (XRD) was used to characterize these carbon products. Figure 2a shows the XRD patterns of chitin as well as those of NC-400, NC-600, NC-800, and NC-1000. The peaks at $2\theta = 19.1$ and 9.1°, representing the (101) and (020) diffraction facets of chitin,[22] disappeared after carbonization at different temperatures. One new peak located at $2\theta = 24.8°$ was ascribed to the diffraction of the (002) facets, which indicated that there was interlayer structure in the material.[23] A second, weak peak appeared at $2\theta = 42.9°$ corresponding to the in-plane diffraction of (100) facets, which reflected the triperiodic order of materials and the formation of a real graphitic phase.[23b,24] According to the XRD patterns, the product achieved at the lowest temperature (400 °C) had already fully lost the crystal structure of chitin and showed some degree of layered structure (broad peak at around 24.8°). With the increase of carbonization temperature, the peak at about 24.8° became sharper, and the peak at about 42.9° became more prominent. It illustrated that the carbon product achieved at higher carbonization temperature has a more regular layered structure and structural order than that obtained at lower temperature.[23b] Consistently, FTIR spectra exhibit systematic changes (Figure 2b). For NC-800 and NC-1000, the characteristic peaks of chitin located at approximately 3260, approximately 1650, 1558, and 1080 cm^{-1}, which were ascribed to the ν_{N-H}, $\nu_{C=O}$, ν_{C-N}, and ν_{C-O} stretching vibrations,[22] disappeared and were replaced by two new vibration peaks located at approximately 1560 and 1120 cm^{-1}, respectively, which corresponded to the vibration of the sp^2 C=N and/or aromatic C=C (1560 cm^{-1}), and sp^3 C–N (1120 cm^{-1}).[25] For NC-400, a weak peak located at approximately 3360 cm^{-1} can be observed, which indicates some primary amine groups may exist.[26]

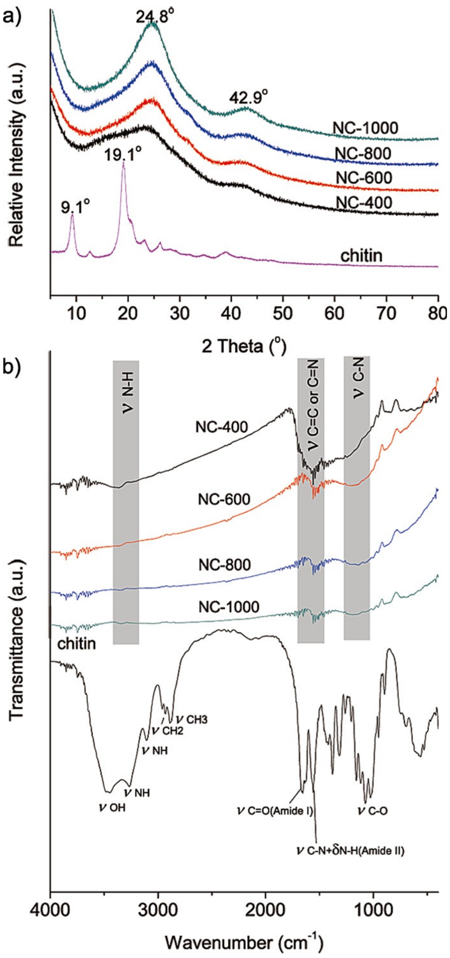

Figure 2. (a) XRD patterns and (b) FTIR spectra of chitin, NC-400, NC-600, NC-800, and NC-1000.

Raman spectroscopy was also used to analyze the microscopic structure of the products, and the original spectra were deconvoluted (Figure 3). Two characteristic Raman bands for graphite, located at approximately 1330 cm^{-1} (D band) and approximately 1575 cm^{-1} (G band),[27] indicated the existence of a graphitic sp^2-hybridized carbon structure in all samples. It is well known that the G band is due to the single-crystal graph-

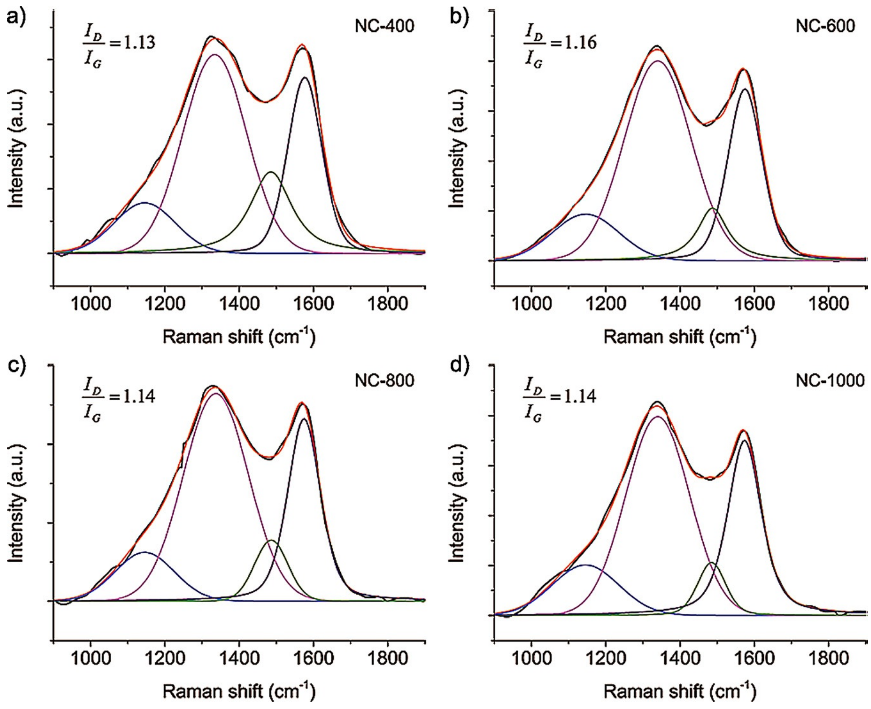

Figure 3. Deconvoluted Raman spectra of (a) NC-400, (b) NC-600, (c) NC-800, and (d) NC-1000.

ite and the D band results from the defects or the polycrystalline graphite in the bulk carbon. The relative intensity of the D band to the G band, I_D/I_G, was usually used as a criterion to determine the disordered extent in carbon materials.[28] The ratio of I_D/I_G for NC-600 was slightly greater than the one for NC-400, which suggested that more defects or a more disordered graphite structure was generated at higher temperature. We deduced that the defects may be formed during the transformation of surface functional groups, such as from amino groups (NH_2) to quaternary nitrogen atoms, which partly destroyed the sp^2-hybridized carbon structure. NC-800 and NC-1000 have the same value of I_D/I_G, slightly smaller than that of NC-600 though, which indicates an increase of the graphitic structure at higher carbonization temperature.

The scanning electron microscopy (SEM) images of NC-400, NC-600, NC-800, and NC-1000 are shown in Figure 4. Compared with chitin, which has a fibrous structure (see Figure S1a in the Supporting Information), the four N-containing carbon materials exhibit a graphitic structure. For NC-400 and NC-600, layered carbon sheets with pores can be observed clearly. For samples carbonized at higher temperatures (NC-800 and NC-1000), the layered carbon sheet is still the predominant structure but the pore size appears to be smaller. These structural features can also be observed in lower magnification SEM images (Figure S2). TEM images provided in Figures S1b and S3 corroborate the layered carbon sheet structure for the NC-600 and NC-800 samples.

Nitrogen-adsorption experiments further demonstrated that these materials have a high surface area and mesoporous structure. Except for NC-1000, all of the isotherms exhibited an unclosed hysteresis loop with the desorption curve lying above the adsorption line (Figure 5a, c, e, and g). This phenomenon was previously observed in some carbonizated high-molecular polymers and was ascribed to a complex “throat- or cavity-type” microporous structure, or to the property of sorbate-induced swelling of micropores.[29] Plausibly, the N-containing carbon materials derived from chitin contained some complex microporous structures, which inhibited the nitrogen contained in the complex-micropore desorption at low relative pressure. All these isotherms belong to the type IV isotherm, which confirms these N-containing carbon materials have a mesoporous structure. Compared with chitin, which has a surface area of merely 7.4 m^2 g^{-1}, the Brunauer–Emmett–Teller (BET) surface areas of NC-400 and NC-600 are much higher, at 221 and 251 m^2 g^{-1}, respectively. At higher carbonization temperatures, the surface area of the product began to decrease. The BET surface area of NC-800 is 181 m^2 g^{-1} and that of NC-1000 is only 18 m^2 g^{-1}, which indicates that some pore structures were damaged at higher carbonization temperature. The pore-size distribution based on Barrett–Joyner–Halenda (BJH) analysis (Figure 5b, d, f, and h) suggested that the pores have already been created at 400 °C, in the range of 2–9 nm and centered at approximately 3.3 nm. Although the surface area exhibited no significant change among samples treated between 400 and 800 °C, the pore-size distribution varied along with the increase of temperature. For NC-600 and NC-800, the pore sizes were randomly distributed in the range of 2–9 nm. In contrast, the porous structure was almost entirely damaged for NC-1000. We also observed the existence of micropores (< 2 nm)

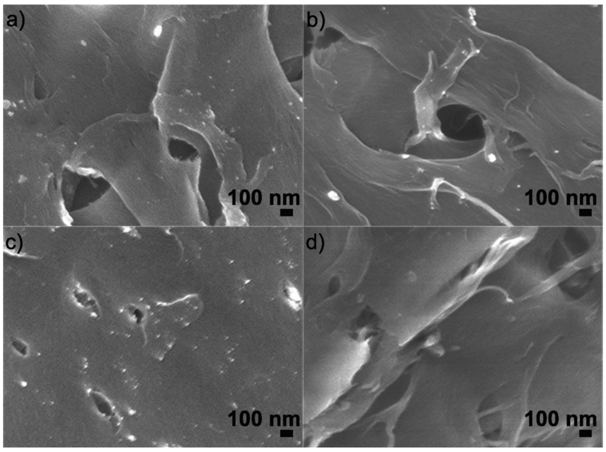

Figure 4. SEM images of (a) NC-400, (b) NC-600, (c) NC-800, and (d) NC-1000.

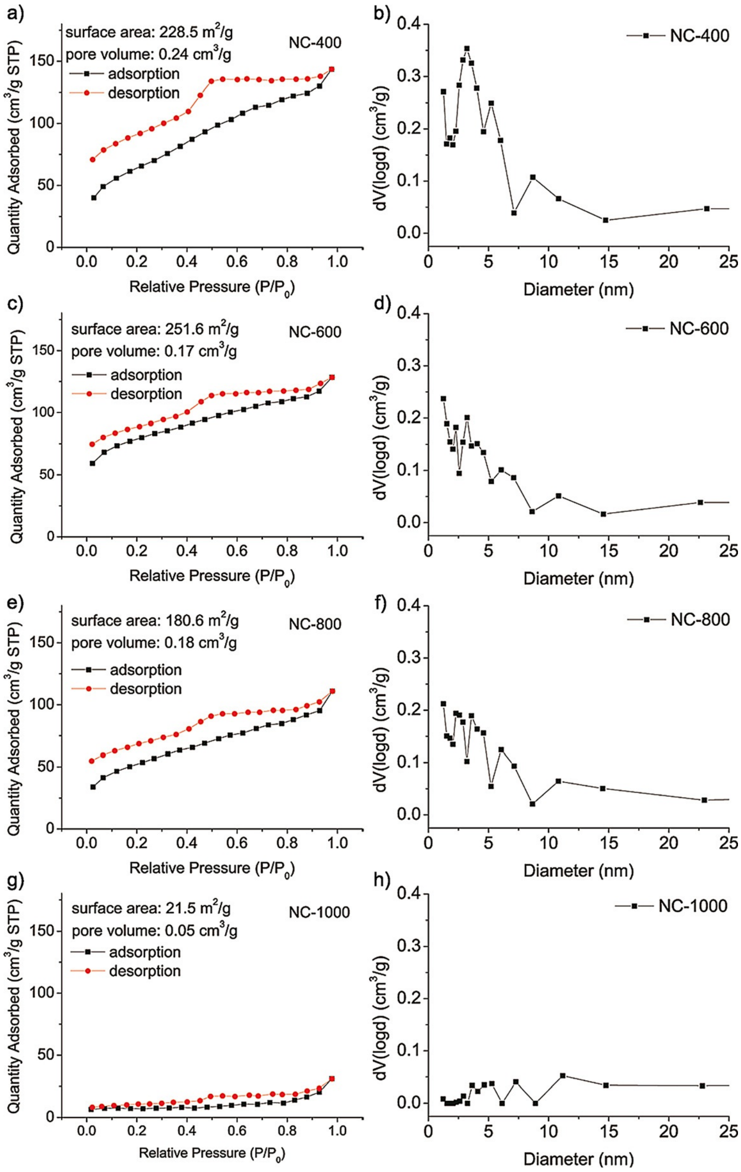

Figure 5. Nitrogen-adsorption isotherms of N-containing carbon: (a) NC-400, (c) NC-600, (e) NC-800, (g) NC-1000, and the pore-size distribution based on BJH analysis of adsorption isotherm data: (b) NC-400, (d) NC-600, (f) NC-800, (h) NC-1000.

in NC-400, NC-600, and NC-800, which further suggest the existence of micropores in the N-containing carbon materials. On considering the TG-IR analysis, most volatile products were generated from the decomposition of chitin at around 400 °C. Plausibly, the large amount of vapor (78 wt % of the starting material) is responsible for the creation of the mesopores when escaping from the bulky solid.

To clarify the changes of the electronic state of nitrogen and carbon atoms in chitin after carbonization, the C 1s and N 1s XPS spectra were collected and analyzed in detail (Figure 6). The C 1s XPS spectra shown in Figure 6a, c, e, and g were deconvoluted to at least five components at 284.9, 285.8, 286.7, 287.6, and 289.2 eV attributed to sp^2 C, C–N, C–O, C=O, and C(O)OH, respectively.[27,30] Among these peaks, the peak at 284.9 eV was the main peak and gradually became sharp along with the increase of carbonization temperature. This proved that the carbonization occurred even at 400 °C, and the extent of graphitization increased along with increased temperature. The peak at 285.8 eV suggested that there were some N-containing groups on the surface of the materials. Some other carbon atoms bearing oxygen-containing groups located at 286.7, 287.6, and 289.2 eV may have resulted from the partial decomposition of the polysaccharide structure. In addition, in the NC-400 C 1s XPS spectrum, there is another peak at 283.5 eV, which could not be ascribed to any of the above. From the XPS handbook, it appears that it may belong to a carbide carbon, however, considering the extremely low metal content (from inductively coupled plasma atomic emission spectroscopy (ICP-OES) analysis), the peak cannot be ascribed to carbide. We tentatively assign the peak to be the amorphous carbon from partial carbonization of chitin at 400 °C, which can be transformed into graphitized carbon at a higher temperature.[31] For the XPS N 1s spectra shown in Figure 6b, d, f, and h, at least four peaks at 398.6, 400.6, 401.2, and 402.5 eV, which correspond to pyridinic N, pyrrolic N, graphitic N, and nitrogen in oxidation states,[12,18,27,32] were taken into consideration during deconvolution. For NC-400, the N 1s spectrum is much more complex than the other three N-containing carbon materials. Other than the four main nitrogen species, there are other nitrogen species such as amide (400.1 eV), amino (398.8 eV), and other unknown nitride (397.3 eV) forms,[33] which is in accordance with the FTIR analysis revealing the N–H stretching vibration at about 3260 cm^{-1} in NC-400. Along with the increase of carbonization temperature, these complex nitrogen species were incorporated into the framework of the carbonized carbon. Indeed, graphitic N and pyridinic N are the major forms of nitrogen in NC-800 and NC-1000. XPS analysis confirmed that not only the nitrogen content, but also the types of major nitrogen species, can be modified by changing the carbonization temperature. A detailed component distribution of carbon and nitrogen types based on XPS fitting results is provided in Table S1 in the Supporting Information.

Heavy-metal adsorption

Mesoporous carbon materials are usually used as adsorbents to remove contaminants from water.[34] We expect our N-containing carbon materials from chitin to be superior in heavy-metal removal from water owing to the strong binding effect between nitrogen and metal ions. To evaluate the metal-removal effect of N-containing carbon materials prepared at different temperatures, three sample solutions containing a kind of metal ion at a concentration of 10 ppm were treated in the presence of NC-400, NC-600, NC-800, and NC-1000, respectively, over a period of 12 hours with stirring (Figure 7a). The adsorption capabilities of N-containing carbon materials for these

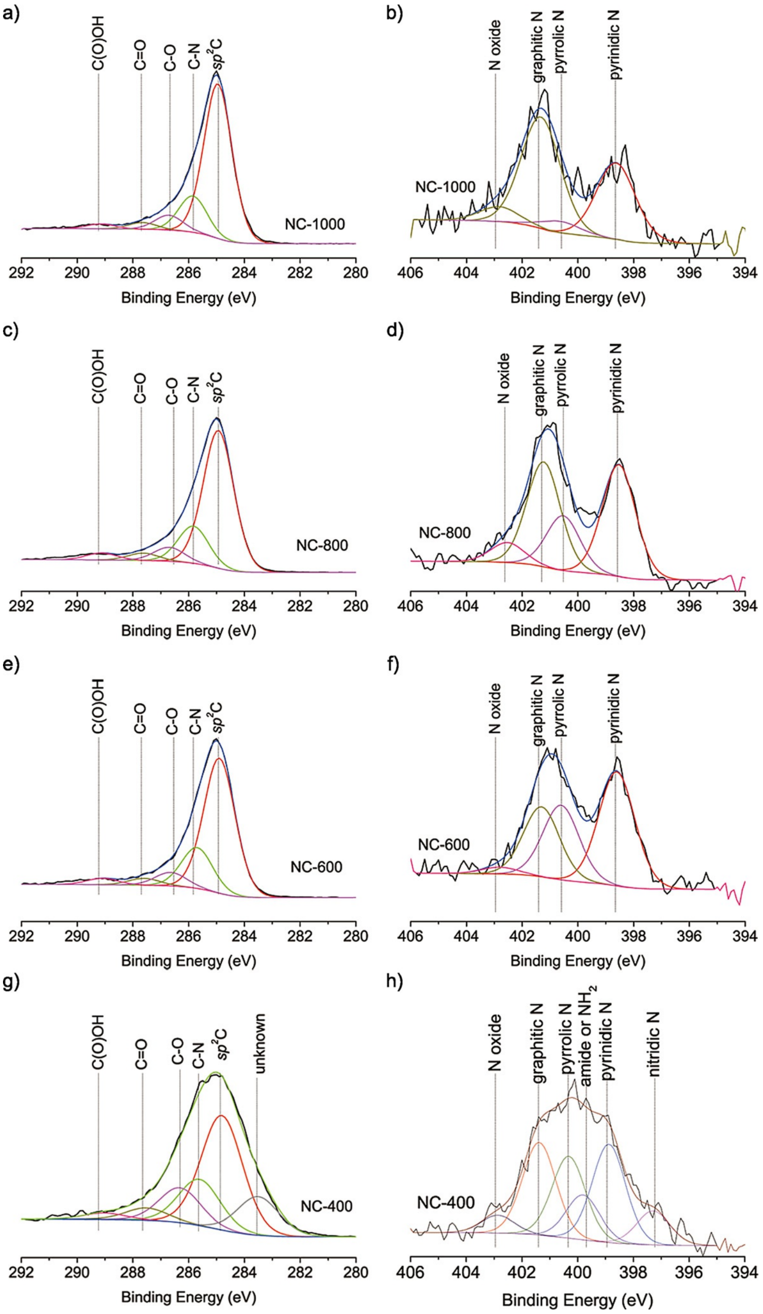

Figure 6. XPS C 1s spectra of N-containing carbon (a) NC-1000, (c) NC-800, (e) NC-600, (g) NC-400, and XPS N 1s spectra of (b) NC-1000, (d) NC-800, (f) NC-600, (h) NC-400.

three heavy-metal ions followed the order of $Hg^{II} > Pb^{II} > Cr^{VI}$. It is clear that the temperature at which the N-containing carbon material is produced has a strong effect on the adsorption ability. NC-400 exhibited the highest capability to remove heavy-metal ions, and the capability dropped monotonically as the carbonization temperature increased. NC-1000 exhibited almost no ability to remove these heavy-metal ions. From these, we conclude that the amino groups and pyrrolic N in the NC material are mainly responsible for the excellent heavy-metal removal, as XPS and IR analysis indicated that the degree of NH_2 and pyrrolic groups in NC dropped with increasing carbonization temperature.

NC-400 was selected for further evaluation. The effect of pH on Cr^{VI} adsorption is shown in Figure 7b. Interestingly, the adsorption ability towards Cr^{VI} is higher at a lower pH. For example, at pH 3.0, the removal efficiency for Cr^{VI} is 92% whereas at pH 10.0, NC-400 almost completely lost its capability to remove Cr^{VI}. This can be rationalized by considering the surface charge state of NC-400 at different pH. Amino groups and other nitrogen species would be protonated at lower pH so that the adsorbent is positively charged. Under this condition, Cr^{VI} ions exist either in the form of $HCrO_4^-$ or CrO_4^-. The electrostatic attractions between the adsorbent and Cr^{VI} anion species enhanced the adsorption efficiency of Cr^{VI} on NC-400. Figure 7c shows the time profile of Cr^{VI} adsorption on NC-400 under neutral conditions. The adsorption amount (q) increased with the adsorption time and reached adsorption equilibrium after five hours. This indicates NC-400 exhibited relatively fast adsorption kinetics in Cr^{VI} removal, comparable with other materials.[35] The adsorption isotherms of Cr^{VI} is illustrated in Figure 7d, at the initial metal-ion concentration of 1–100 ppm. The q_e reached a remarkable 47.8 mg g^{-1}, at a Cr^{IV} equilibrium concentration of 88 ppm (which corresponds to a 100 ppm initial concentration), which is considerably larger than the data achieved by other adsorbents such as sawdust (3.3 mg g^{-1}),[36] chitosan cross-linked with epichlorohydrin (11.3 mg g^{-1}),[37] and magnetic graphene (4.9 mg g^{-1}),[35a] under similar conditions, which indicates that NC-400 is a very promising material in the preconcentration and/or removal of heavy-metal ions from aqueous solutions.

Catalytic activity

It is well established that N-doped carbon materials exhibit excellent catalytic oxidation activity because the doped nitrogen can impact the electronic state of carbon.[12,38] As such, we carried out preliminary tests on the catalytic activity of chitin-derived N-containing carbon materials in the epoxidation of styrene using *tert*-butyl hydroperoxide (TBHP) as the oxidant. Indeed, these materials effectively promoted the oxidation reaction. In the absence of catalyst the conversion is very low (2.7%) with only 2 mol% of epoxide obtained after one hour (Table 2, entry 1). When 10 mg NC-400 was used, both the styrene conversion and epoxide yield increased considerably (Table 2, entries 2–5). Among the four N-containing carbon materials, NC-1000 exhibits the highest catalytic activity; whereas NC-400 exhibited the worst catalytic activity under the same reaction conditions. The performances of NC-600 and NC-800 were moderate. When the reaction time was prolonged to 12 hours, the conversion of styrene and the yield of styrene increased accordingly. NC-1000 still exhibited the highest catalytic activity (67% conversion) compared to the other three carbon materials, whereas NC-800 and NC-600

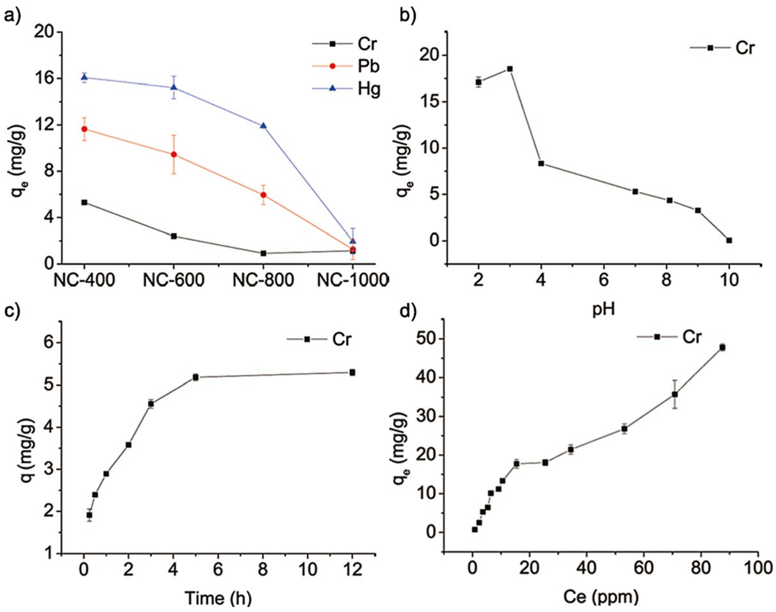

Figure 7. (a) The adsorption ability of N-containing carbon materials for Cr^{VI}, Pb^{II}, and Hg^{II}. (b) The pH effect on Cr^{VI} adsorption by NC-400. (c) The time profile of Cr^{VI} adsorption on NC-400. (d) The adsorption ability of NC-400 for Cr^{VI} at different equilibrium concentrations. Conditions: (a) 5 mg NC, 20 mL solution (pH 7, metal ion concentration = 5 ppm), 12 h, stirring; (b) 5 mg NC-400, 20 mL solution (pH was adjusted by HNO_3 and NaOH, $C_0(Cr^{VI}) = 5$ ppm), 12 h, stirring; (c) 5 mg NC-400, 20 mL solution (pH 7, $C_0(Cr^{VI}) = 5$ ppm), stirring; (d) 5 mg NC-400, 20 mL solution (pH 7, $C_0(Cr^{VI}) = 1–100$ ppm,), stirring. C_e is the equilibrium concentration of Cr^{VI}. q_e [mg g^{-1}] is the equilibrium amount of heavy metal adsorbed per gram of adsorbent.

Table 2. Catalytic activity of carbon materials in the epoxidation of styrene.[a]

Entry	Catalyst	t [h]	Conv. [%]	Selectivity [mol %]			
				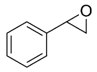	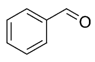	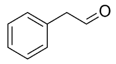	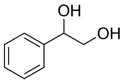
1	none	1	2.7	74.1	22.2	0.0	0.0
2	NC-400	1	5.7	57.9	7.0	1.8	0.0
3	NC-600	1	10.7	53.3	11.2	1.9	0.0
4	NC-800	1	11.2	67.9	11.6	1.8	0.0
5	NC-1000	1	14.9	65.1	10.7	2.0	0.0
6	NC-400	12	29.7	74.4	6.7	1.3	4.0
7	NC-600	12	41.9	87.8	7.2	1.2	1.9
8	NC-800	12	46.1	87.6	5.2	1.1	1.1
9	NC-1000	12	66.8	62.9	6.1	0.7	20.1
10	C-1000	12	19.5	23.1	5.6	1.0	35.9
11[b]	N-OLC-3	4	88.4	46.0	all others 54.0		
12[b]	N-CNTs	4	75.1	11.1	all others 88.9		
13[c]	NG-800	24	87.6	72.8	all others 27.2		

[a] Reaction conditions: styrene 0.5 mmol, catalyst 10 mg, TBHP 1.5 mmol, 3 mL CH_2Cl_2, 100 °C, 1 h, after reaction, 30 mg dodecane was added as an internal standard and products were analyzed by a GC-7890 equipped with a HP-5 column. [b] Ref. [38b]: 90 °C, catalyst 10 mg, styrene/TBHP = 1:3. [c] Ref. [39]: 100 °C, catalyst 10 mg, styrene/TBHP = 1:3.

exhibited the highest selectivity towards epoxide (88%) (Table 2, entries 6–9). The lower selectivity for the NC-1000 catalyst is due to the formation of styrene glycol (20% selectivity). These results indicate that NC-1000 can not only catalyze the epoxidation of styrene but also the hydrolysis of styrene oxide. Therefore, NC-800 is the most suitable catalyst for the reaction among the four N-containing carbon catalysts, which enables the highest yield for the desired product. Compared with other N-containing carbon materials, such as nitrogen-doped onion-like carbon (N-OLC),[38b] nitrogen-doped carbon nanotubes (N-CNTs),[38b] and N-doped graphene,[39] the catalytic activity of the N-containing carbon derived from chitin was slightly lower but the selectivity to styrene oxide was higher. To demonstrate the function of nitrogen atoms in the material for catalysis, a nitrogen-free carbon material was prepared by carbonizing microcrystalline cellulose at 1000 °C (termed as C-1000). The poor catalytic activity and low selectivity for epoxide were observed under the same reaction conditions (Table 2, entry 10). Combining the XPS fitting results with the reaction performances, it is clear that the surface area and the nitrogen content are not the determining factors for a superior catalytic activity. The content of graphitic carbon and graphitic nitrogen are plausibly the main factors responsible for styrene epoxidation. Therefore, the higher carbonization temperature is critical to achieve a kind of N-containing carbon material with excellent catalytic activity for oxidation reactions. Although more active carbon-based catalysts are known, including in epoxidation,[39] the simple procedure for the catalyst synthesis from an abundant, renewable material makes chitin-derived NC attractive for catalytic applications.

Conclusion

In conclusion, a simple, scalable, and affordable carbonization method, in the absence of any additional reagent, for the preparation of mesoporous, N-containing carbon materials from chitin was developed. The pore structure, surface area, and types of nitrogen in the resulting material can be easily adjusted by changing the carbonization temperature, leading to materials suitable for different applications. A low carbonization temperature is beneficial to achieve a carbon material with large surface area and high nitrogen content enriched with amine and pyrrolic functionalities, which are beneficial to the removal of heavy-metal ions from water. In contrast, a higher carbonization temperature increases the content of graphitic nitrogen and carbon, which are essential for excellent catalytic activity in oxidation reactions such as styrene epoxidation. This study highlights the potential of utilizing chitin, the second most abundant biomaterial on earth, to manufacture functionalized N-containing carbon materials. More applications of these novel carbon materials as catalysts, adsorbents, and beyond are currently under development in the group.

Experimental Section

Chemicals

α-Chitin was purchased from Wako Pure Chemical Industry. Styrene (≥99%), 4-*tert*-butylhydroperoxide solution (TBHP, 70 wt% in water), $HgCl_2$ (ACS reagent, ≥99.5%), and dodecane (≥99%) were purchased from Sigma–Aldrich. $K_2Cr_2O_7$ (≥99.9%) was produced by Fisons Scientific Equipment. Dichloromethane (analytical reagent grade) was produced by Fisher Scientific Company. $Pb(NO_3)_2$ was purchased from Merck Chemicals. All chemicals were used without further treatment.

Characterization

XPS spectra were recorded on a VG ESCALAB 220I-XL system equipped with two types of X-ray sources: the twin anode (Mg/Al) and the twin-crystal monochromated Al source, producing spectra from areas ranging from 8 mm down to 20 mm in diameter. The data were calibrated by the C 1s signal (285.0 eV) and processed further. XRD analysis was carried out on a Bruker D8 Advanced diffractometer using $Cu_{K\alpha}$ ($\lambda = 1.5406$ Å) radiation (40 kV voltage, 30 mA cathodic current). Diffraction patterns were recorded within a 2θ range of 5–80°. SEM images were taken with a JSM-6700F field-emission microscope. The carbon materials powder was directly immobilized on a copper holder by conducting resin without platinum coating before characterization. TEM images were taken on a JEOL JEM-2010 microscope. The samples were dispersed in ethanol by ultrasonication and then dropped on a copper grid. Gas sorption isotherms were measured using a Nova 4200e surface-area analyzer. The materials were degassed at 150 °C for at least 17 hours. The BET specific surface areas were calculated by using the adsorption data in the relative pressure (P/P_0) range of 0.05–0.35. The pore-size distribution for each sample was based on BJH analysis of adsorption isotherm data. FTIR were achieved on a Bruker Equinox 55 infrared spectrometer. The number of scans was 16 with a resolution of 4 cm^{-1} over the range of 4000–400 cm^{-1} under transmittance mode. A sample (about 2 mg) was diluted by KBr (98 mg) and then pressed into a wafer before measurement. Thermogravimetric analysis was conducted on a DTG-60A thermogravimetry analyzer (Shimadzu) under a nitrogen atmosphere and the volatile products were detected by a coupled Fourier transform infrared spectrophotometer (IR Prestige-21, Shimadzu) online. Raman analysis was conducted on an XploRA PLUS Raman microscope (Horiba/JY, France). The samples were placed on a glass slide and measured directly. All spectra were obtained with a laser wavelength of 532 nm and laser power of 25 mW. The scan range was between 500 and 3500 cm^{-1} and the scan time was 60 seconds. All the original Raman spectra had their linear background subtracted and deconvoluted by using PeakFit version 4.12 software. The range of the processed spectrum was 900–2000 cm^{-1} with the best baseline mode and Gaussian–Lorentzian area mode with a multipeak best fit. The deconvoluted peaks at approximately 1330 and approximately 1575 cm^{-1} along with the D and G bands and the ratios of the two peak intensities were calculated based on the height of the two deconvoluted peaks.

Protocols for preparing N-containing carbon from chitin

Chitin (1 g) was loaded into a quartz tube that was placed in a tubular furnace and nitrogen gas with the flow rate of 50 mL min^{-1} was connected. The furnace was heated at a rate of 10 °C min^{-1} from room temperature to the target temperature. Then the furnace was held at this temperature for 4 hours before cooling down. The liquid product was collected in a two-necked flask (10 mL) connected to one end of the quartz tube, cooled by air. The quartz tube was taken out the furnace and the product in the tube was collected and analyzed further.

Quantification of calcium in chitin

Chitin (0.0512 g) was digested in concentrated nitric acid (65 wt%, 10 mL) at 120 °C for 12 hours. The solution was transferred to a volumetric flask (25 mL) and the flask was topped up to the mark line by the addition of pure water. Then the solution was analyzed by ICP-OES.

GC-MS and GC analysis of liquid products

The liquid products generated during the carbonization process were analyzed and quantified by the pre-column derivatization method, by employing hexamethyldisililazane to silylate the hydroxyl groups.[40] The liquid product (0.1 g), a small magnetic stirring bar, and derivatization reagents, including pyridine (1.5 mL), hexamethyldisilazane (1.5 mL), and trifluoroacetic acid (0.1 mL), were added into a small flask (10 mL). The flask was sealed and heated under stirring in a water bath at 60 °C for 1 h. After silylation, dedecane (8 mg) was added into the system and the mixture was analyzed on a GC-MS (Agilent 7890A GC system with a 7693 Autosampler, 5975C inert MSD with triple-axis detector, and an Agilent HP-5 column). After the structures of all the peaks were determined on a GC-MS spectrum, the sample was analyzed further and quantified on a GC (Agilent 7890) equipped with a FID detector.

Adsorption of Cr^{VI}, Pb^{II}, and Hg^{II} by N-containing carbon materials

Stock solutions (100 ppm) of Cr^{VI}, Pb^{II}, and Hg^{II} were prepared in ultrapure water. In the experiments, heavy-metal solutions (20 mL, 1–20 ppm) were prepared by diluting the stock solution and then the N-containing carbon material (5 mg) was added. Then the solution was stirred by a magnetic stirring bar at 1000 rpm for 0.25–12 hours. At the end of the adsorption, the adsorbent was removed by filtration and the solution was acidified by nitrate acid and analyzed by ICP-OES. All adsorption experiments were carried out in triplicate and the results were presented in the form of average values and relative percentage deviations. The amount of the heavy metals adsorbed per unit mass of adsorbent was calculated according to Equation (1):

$$q_e = (C_0 - C_f)V/M \qquad (1)$$

in which q_e [mg g^{-1}] is the adsorption amount of heavy metal per mass of adsorbent, C_0 and C_f are the initial and final concentration [ppm] of heavy metal ions, respectively, V is solution volume [mL], and M is the mass of adsorbent [g].

Catalytic activity evaluation

The catalytic activity evaluation was conducted in a thick-walled glass tube equipped with a Teflon lid. In general, N-containing carbon materials (10 mg), styrene (1 mmol), CH_2Cl_2 (2 mL), and TBHP (460 μL) were added into the reaction tube in turn. Then the tube was sealed with the Teflon lid and placed into a metal heater at 100 °C for 1 or 12 hours. After the reaction, dodecane (30 mg) was added as an internal standard and dichloromethane (5 mL) was added as the dilution solvent. After filtration, the solution was analyzed by a Agilent 7890 gas chromatograph equipped with HP-5 capillary column and flame ionization detector, and then the conversion of styrene and the yields of the products were calculated according to the peak area and calibration curve.

Acknowledgements

*This study was financially supported by A*Star, PSF funding through WBS: R-279-000-403-305. We thank Michael Joyes for the proofreading.*

Keywords: adsorption · biomass · carbohydrates · epoxidation · mesoporous materials

[1] a) J. Lee, J. Kim, T. Hyeon, *Adv. Mater.* **2006**, *18*, 2073–2094; b) C. Liang, Z. Li, S. Dai, *Angew. Chem. Int. Ed.* **2008**, *47*, 3696–3717; *Angew. Chem.* **2008**, *120*, 3754–3776; c) T.-Y. Ma, L. Liu, Z.-Y. Yuan, *Chem. Soc. Rev.* **2013**, *42*, 3977–4003; d) R. J. White, V. Budarin, R. Luque, J. H. Clark, D. J. Macquarrie, *Chem. Soc. Rev.* **2009**, *38*, 3401–3418.

[2] Y. Li, J. Fu, S. Deng, X. Lu, *J. Colloid Interface Sci.* **2014**, *424*, 104–112.

[3] P. Xu, D. Wu, L. Wan, P. Hu, R. Liu, *J. Colloid Interface Sci.* **2014**, *421*, 160–164.

[4] L. Schlapbach, A. Zuttel, *Nature* **2001**, *414*, 353–358.

[5] F. Rodríguez-Reinoso, *Carbon* **1998**, *36*, 159–175.

[6] a) S. Navalon, A. Dhakshinamoorthy, M. Alvaro, H. Garcia, *Chem. Rev.* **2014**, *114*, 6179–6212; b) W. J. Lee, U. N. Maiti, J. M. Lee, J. Lim, T. H. Han, S. O. Kim, *Chem. Commun.* **2014**, *50*, 6818–6830; c) P. Chen, T. Y. Xiao, Y. H. Qian, S. S. Li, S. H. Yu, *Adv. Mater.* **2013**, *25*, 3192–3196.

[7] a) J. S. Lee, X. Wang, H. Luo, G. A. Baker, S. Dai, *J. Am. Chem. Soc.* **2009**, *131*, 4596–4597; b) S. Zhang, K. Dokko, M. Watanabe, *Chem. Mater.* **2014**, *26*, 2915–2926.

[8] T.-D. Nguyen, K. E. Shopsowitz, M. J. MacLachlan, *J. Mater. Chem. A* **2014**, *2*, 5915–5921.

[9] H. Zhong, H. Zhang, S. Liu, C. Deng, M. Wang, *ChemSusChem* **2013**, *6*, 807–812.

[10] H.-g. Wang, Z. Wu, F.-l. Meng, D.-l. Ma, X.-l. Huang, L.-m. Wang, X.-b. Zhang, *ChemSusChem* **2013**, *6*, 56–60.

[11] X. L. Li, H. L. Wang, J. T. Robinson, H. Sanchez, G. Diankov, H. J. Dai, *J. Am. Chem. Soc.* **2009**, *131*, 15939–15944.

[12] Y. Gao, G. Hu, J. Zhong, Z. Shi, Y. Zhu, D. S. Su, J. Wang, X. Bao, D. Ma, *Angew. Chem. Int. Ed.* **2013**, *52*, 2109–2113; *Angew. Chem.* **2013**, *125*, 2163–2167.

[13] J. H. Clark, *Nat. Chem.* **2009**, *1*, 12–13.

[14] K. W. Buck, M. A. Obaidah, *Biochem. J.* **1971**, *125*, 461–471.

[15] a) E. Khor, L. Y. Lim, *Biomaterials* **2003**, *24*, 2339–2349; b) M. Rinaudo, *Prog. Polym. Sci.* **2006**, *31*, 603–632.

[16] F. M. Kerton, Y. Liu, K. W. Omari, K. Hawboldt, *Green Chem.* **2013**, *15*, 860–871.

[17] a) Y. Pierson, X. Chen, F. D. Bobbink, J. Zhang, N. Yan, *ACS Sustainable Chem. Eng.* **2014**, *2*, 2081–2089; b) X. Chen, S. L. Chew, F. M. Kerton, N. Yan, *Green Chem.* **2014**, *16*, 2204–2212; c) X. Chen, N. Yan, *Catal. Surv. Asia* **2014**, 1–13; d) K. W. Omari, J. E. Besaw, F. M. Kerton, *Green Chem.* **2012**, *14*, 1480–1487; e) F. D. Bobbink, J. Zhang, Y. Pierson, X. Chen, N. Yan, *Green Chem.* **2015**, *17*, 1024–1031; f) X. Chen, Y. Liu, F. M. Kerton, N. Yan, *RSC Adv.* **2015**, *5*, 20073–20080.

[18] R. J. White, M. Antonietti, M. M. Titirici, *J. Mater. Chem.* **2009**, *19*, 8645–8650.

[19] L. Wang, Y. L. Zheng, X. H. Wang, S. H. Chen, F. G. Xu, L. Zuo, J. L. Wu, L. L. Sun, Z. Li, H. Q. Hou, Y. H. Songt, *ACS Appl. Mater. Interfaces* **2014**, *6*, 7117–7125.

[20] M. Zhang, L. Shu, X. F. Shen, X. Y. Guo, S. Tao, B. S. Xing, X. L. Wang, *Environ. Pollut.* **2014**, *195*, 84–90.

[21] D. Wang, R. Xiao, H. Zhang, G. He, *J. Anal. Appl. Pyrolysis* **2010**, *89*, 171–177.

[22] G. Cárdenas, G. Cabrera, E. Taboada, S. P. Miranda, *J. Appl. Polym. Sci.* **2004**, *93*, 1876–1885.

[23] a) A. Primo, A. Forneli, A. Corma, H. García, *ChemSusChem* **2012**, *5*, 2207–2214; b) L. Zhao, N. Baccile, S. Gross, Y. Zhang, W. Wei, Y. Sun, M. Antonietti, M.-M. Titirici, *Carbon* **2010**, *48*, 3778–3787.

[24] a) K. S. Subrahmanyam, S. R. C. Vivekchand, A. Govindaraj, C. N. R. Rao, *J. Mater. Chem.* **2008**, *18*, 1517–1523; b) L. Yu, C. Falco, J. Weber, R. J. White, J. Y. Howe, M.-M. Titirici, *Langmuir* **2012**, *28*, 12373–12383; c) Q. Zhao, T.-P. Fellinger, M. Antonietti, J. Yuan, *J. Mater. Chem. A* **2013**, *1*, 5113–5120.

[25] a) T. V. Khai, H. G. Na, D. S. Kwak, Y. J. Kwon, H. Ham, K. B. Shim, H. W. Kim, *J. Mater. Chem.* **2012**, *22*, 17992–18003; b) H. Kaczmarek, J. Zawadzki, *Carbohydr. Res.* **2010**, *345*, 941–947.

[26] a) T. Ramanathan, F. T. Fisher, R. S. Ruoff, L. C. Brinson, *Chem. Mater.* **2005**, *17*, 1290–1295; b) M. H. Ahmed, J. A. Byrne, J. A. D. McLaughlin, A. Elhissi, W. Ahmed, *Appl. Surf. Sci.* **2013**, *273*, 507–514.

[27] P. Hao, Z. Zhao, Y. Leng, J. Tian, Y. Sang, R. I. Boughton, C. P. Wong, H. Liu, B. Yang, *Nano Energy* **2015**, *15*, 9–23.

[28] A. C. Ferrari, J. Robertson, *Phys. Rev. B* **2000**, *61*, 14095–14107.

[29] a) P. M. Budd, A. Butler, J. Selbie, K. Mahmood, N. B. McKeown, B. Ghanem, K. Msayib, D. Book, A. Walton, *Phys. Chem. Chem. Phys.* **2007**, *9*, 1802–1808; b) F. J. Liu, C. J. Li, L. M. Ren, X. J. Meng, H. Zhang, F. S. Xiao, *J. Mater. Chem.* **2009**, *19*, 7921–7928.

[30] S. Stankovich, D. A. Dikin, R. D. Piner, K. A. Kohlhaas, A. Kleinhammes, Y. Jia, Y. Wu, S. T. Nguyen, R. S. Ruoff, *Carbon* **2007**, *45*, 1558–1565.

[31] J. Nakamura, I. Toyoshima, K.-i. Tanaka, *Surf. Sci.* **1988**, *201*, 185–194.

[32] S. Biniak, G. Szymanski, J. Siedlewski, A. Swiatkowski, *Carbon* **1997**, *35*, 1799–1810.

[33] a) H. P. Mungse, O. P. Khatri, *J. Phys. Chem. C* **2014**, *118*, 14394–14402; b) A. M. Alswieleh, N. Cheng, I. Canton, B. Ustbas, X. Xue, V. Ladmiral, S. J. Xia, R. E. Ducker, O. El Zubir, M. L. Cartron, C. N. Hunter, G. J. Leggett, S. P. Armes, *J. Am. Chem. Soc.* **2014**, *136*, 9404–9413; c) J. F. Moulder, W. F. Stickle, P. E. Sobol, K. D. Bomben, *Handbook of X Ray Photoelectron Spectroscopy: A Reference Book of Standard Spectra for Identification and Interpretation of XPS Data (Edited by Jill Chastain) PerkinElmer Coporation Physical Electronic Division* **1992**, p. 43.

[34] A. Muñoz García, A. J. Hunt, V. L. Budarin, H. L. Parker, P. S. Shuttleworth, G. J. Ellis, J. H. Clark, *Green Chem.* **2015**, *17*, 2146–2149.

[35] a) G. Gollavelli, C.-C. Chang, Y.-C. Ling, *ACS Sustainable Chem. Eng.* **2013**, *1*, 462–472; b) H. Jabeen, V. Chandra, S. Jung, J. W. Lee, K. S. Kim, S. B. Kim, *Nanoscale* **2011**, *3*, 3583–3585.

[36] H. C. P. Srivastava, R. P. Mathur, I. Mehrotra, *Environ. Technol. Lett.* **1986**, *7*, 55–63.

[37] S. Qian, G. Huang, J. Jiang, F. He, Y. Wang, *J. Appl. Polym. Sci.* **2000**, *77*, 3216–3219.

[38] a) Y. Gao, J. Zhang, X. Chen, D. Ma, N. Yan, *ChemPlusChem* **2014**, *79*, 825–834; b) Y. Lin, X. Pan, W. Qi, B. Zhang, D. S. Su, *J. Mater. Chem. A* **2014**, *2*, 12475–12483; c) Y. Cao, H. Yu, F. Peng, H. Wang, *ACS Catal.* **2014**, *4*, 1617–1625; d) L. Zhao, R. He, K. T. Rim, T. Schiros, K. S. Kim, H. Zhou, C. Gutiérrez, S. P. Chockalingam, C. J. Arguello, L. Pálová, D. Nordlund, M. S. Hybertsen, D. R. Reichman, T. F. Heinz, P. Kim, A. Pinczuk, G. W. Flynn, A. N. Pasupathy, *Science* **2011**, *333*, 999–1003.

[39] W. Li, Y. Gao, W. Chen, P. Tang, W. Li, Z. Shi, D. Su, J. Wang, D. Ma, *ACS Catal.* **2014**, *4*, 1261–1266.

[40] S. H. Langer, S. Connell, I. Wender, *J. Org. Chem.* **1958**, *23*, 50–58.

Manuscript received: June 24, 2015
Revised: July 22, 2015
Final Article published: August 12, 2015